RSC Advances

PAPER

View Article Online
View Journal | View Issue

Cite this: *RSC Adv.*, 2016, **6**, 105607

Resveratrol–ZnO nanohybrid enhanced anti-cancerous effect in ovarian cancer cells through ROS

Mahamuda Khatun,[a] Susobhan Choudhury,[b] Bo Liu,[c] Peter Lemmens,[cd] Samir Kumar Pal*[b] and Santasree Mazumder*[a]

The use of nanotechnology in medicine and more specifically in drug delivery is expected to spread rapidly. Currently many substances are under investigation for drug delivery and more specifically for cancer therapy. Nano-conjugation of the drug is likely to provide protection against degradation, increasing bioavailability, and improvement in intracellular penetration, enhanced efficacy and control delivery of the drug. In this study, ZnO nanoparticles (NPs) conjugated with a well-known anti-proliferative and chemopreventive *trans*-resveratrol (RSV) has been designed, characterized and found to be a potential drug for ovarian cancer treatment. Nano-conjugate (RSV–ZnO) has been characterized by FTIR, Raman scattering and Transmission electron microscopy (TEM). Picosecond-resolved fluorescence studies of RSV–ZnO nano-conjugate reveal efficient electron migration from ZnO NPs to RSV, eventually enhancing the ROS activity compared to free RSV. Various *in vivo* and *in vitro* studies including MTT assay and apoptosis studies on ovarian cancer (PA1) cell lines reveals the RSV–ZnO nano-conjugate to be more effective in cancer cell death in comparison to free RSV. DCFH assay (*in vitro*) and DCFDA method (*in vivo* in PA1 cell lines) demonstrate the huge enhancement of antioxidant property (through ROS) in case of nano-conjugate. JC-1 staining method unravels the increase in depolarization of the mitochondrial membrane in the PA1 cell upon nano-conjugate, consistent with mitochondrial dysfunction. Finally we have performed a Western blot study by expression of some proteins like actin, Bax, Bcl-2 and Caspase-9 to confirm apoptosis.

Received 28th June 2016
Accepted 28th October 2016

DOI: 10.1039/c6ra16664d

www.rsc.org/advances

1. Introduction

Ovarian cancer is the most common cause of cancer mortality in women and one of the leading reasons for death from gynaecological malignancies.[1,2] In the case of maximum patients, the early stage of malignancy is rarely detected and symptoms are evident after spreading out over the surface of the peritoneal cavity. While patients with early-stage cancer have a survival rate of 90%, advanced-stage patients have a survival rate of 15% to 30% only.[3] Conventional approaches like chemotherapy[4] and cytoreductive surgery have limited success of controlling ovarian cancer due to chemotherapy resistance and a high recurrence rate.[5] Resveratrol (3,5,4′-trihydroxy-*trans*-stilbene), the natural phytoalexin present in grapes, berries, peanuts and red wine, is well known for its antioxidant,[6] antiaging,[7] antivira cardiovascular and neuro protective effectsl.[8] Several recent studies demonstrated antiproliferative, anticancer and chemopreventive efficacy of resveratrol (RSV) against of a wide variety of tumors including breast,[9] prostate,[10] lymphoid,[11] lung,[12] pancreas,[13] colon[14] cervical[15] and ovarian[16] cancer. RSV is believed to directly modulate various molecular signal transduction pathways that are known to inhibit cancer cell proliferation and induce cancer cell death.[17] In some lineages of cancer cell culture, RSV has been shown to induce apoptosis, revealing RSV is responsible for cancer cell death through antioxidant and anti-angiogenic properties.

Regardless of the promising results reported in the contemporary literature, the massive use of RSV has met limited success due to its instability, poor solubility in water, inefficient systemic delivery, and low bioavailability.[18–20] To overcome these physicochemical and pharmacokinetic limitations, the conjugation of RSV with nanoparticles (NPs) is a powerful strategy.[21] Zinc oxide (ZnO) NPs is receiving much attention for their good effectiveness in cancer treatment[22] and also for potential targeted drug delivery. It has also been reported that ZnO NPs selectively induce apoptosis in human cancer cells through reactive oxygen species (ROS).[23] ZnO NPs are being

[a]*Department of Biochemistry, Ballygunge Science College, University of Calcutta, Kolkata 700 019, India. E-mail: smbioc@gmail.com*

[b]*Department of Chemical, Biological & Macromolecular Sciences, S. N. Bose National Centre for Basic Sciences, Block JD, Sector III, Salt Lake, Kolkata 700106, India. E-mail: skpal@bose.res.in*

[c]*Institute for Condensed Matter Physics, TU-Braunschweig Mendelssohnstrasse 3, 38106 Braunschweig, Germany*

[d]*Laboratory for Emerging Nanometrology, TU-Braunschweig Mendelssohnstrasse 3, 38106 Braunschweig, Germany*

used in the food industry as additives and in packaging due to their antimicrobial properties.[24,25] They are also being explored for their potential use as anticancer drugs and biomedical imaging applications.[26,27] In mammalian cells, the toxic effects of ZnO NPs such as membrane injury, inflammatory response, DNA damage and apoptosis have been demonstrated.[28–30] In some studies, the toxicity of ZnO NPs has been ascribed to the release of Zn^{2+} ions.[31,32] However, studies have also shown that the toxicity of ZnO NPs is due to their particulate nature which may give rise to reactive oxygen species.[29,33] ROS generation is linked to DNA damage and cellular apoptosis.[34,35] By using the advantage of particulate nature of ZnO NPs we design our research work by forming conjugation of ZnO and resveratrol. The treatments available are limited and most of them have toxic/adverse effect. When the cancer is metastasized, the treatment options are limited, and chemotherapy remains the only choice of treatment. So it raises a large scope of research on natural and nontoxic anticancer agents. To convey higher therapeutic payload to the cells, compared to the RSV molecules, the nanoconjugate of ZnO–RSV is synthesized.

To continue our research focused on the use of natural phenol compounds on ovarian cancer, in this study we have investigated the ZnO–RSV nano-conjugate as a potential drug for ovarian cancer treatment on PA1 cell lines. To explore and modulate the effectiveness of NPs, RSV–ZnO nano-conjugates have been prepared by conjugation of ZnO NPs of ~5 nm particle size and RSV drug molecules. Small size of the ZnO–RSV is very effective in interacting with cells. The nano-conjugates have been characterized by different optical techniques. The sizes of the NPs and crystallinity were confirmed using high-resolution transmission electron microscopy (HRTEM). FTIR and Raman scattering studies were used to understand the conjugation at the molecular level. Steady-state fluorescence and picosecond resolved fluorescence studies unravel the efficient electron transfer from ZnO to RSV, which probably increase the ROS activity in the nano-conjugate. From our studies it is clearly visible that upon conjugation with ZnO NPs the ROS activity of RSV increases drastically compared to free RSV both *in vitro* and *in vivo*. Effective cancer cell death in PA1 cell lines by nano-conjugate compared to free RSV was observed through MTT and flow cytometry (FACS) assays. Western blot assay was performed by expressing Bax Bcl-2, Caspase-9 proteins in PA1 cells in order to confirm the apoptotic pathway of cell death. Depolarization of the mitochondrial membrane in the PA1 cell was also observed using JC-1 staining method. Overall, our present study is an attempt to explore the enhanced anti-cancer activity of the promising nano-conjugate through ROS generation.

2. Materials and methods

2.1. Materials

The PA1 cell line was purchased from National Centre for Cell Science (Pune, India). Resveratrol was from Sigma Aldrich (Saint Louis, MO) and pure zinc acetate dehydrate ($Zn[CH_3COO]_2H_2O$, 99–100%) was from Merck Chemicals (Darmstadt, Germany). Fetal bovine serum (FBS), antibiotic (penicillin–streptomycin), EMEM (Eagle's Minimum Essential Medium) medium and Dulbecco phosphate buffered saline (PBS) were purchased from Invitrogen Co, (Carlsbad, CA). MTT (3-(4,5-dimethylthiazol-2-yl)-2,5-diphenyltetrazoliumbromide), 2,7-dichlorofluorescin diacetate (DCFH-DA), Annexin V/FITC apoptosis detection kit were from BD Bioscience. JC-1 fluorescent probe 5,50,6,60-tetrachloro-1,10,3,30-tetraethylbenzimidazolcarbocyanine iodide, Hoechst and PI stain were from Sigma Aldrich (St Louis, MO). Anti-Caspase, anti-Bax, anti-Bcl-2, and anti-β-actin antibodies were obtained from Sigma-Aldrich (St Louis, MO). Secondary antibodies were bought from Santa Cruz Biotechnology, Inc, (Santa Cruz, CA). All other chemicals used were of the highest purity available from commercial sources.

2.2. Synthesis of ZnO NPs and RSV–ZnO nano-conjugate

ZnO NPs were prepared by the co-precipitation technique using highly pure zinc acetate dehydrate ($Zn[CH_3COO]_2H_2O$, 99% pure) as a precursor with sodium hydroxide solution following the procedures reported earlier.[36] With this ZnO solution required amount of RSV was added into 20 ml of ZnO NPs solution and kept it in a shaker for overnight to formation of nano-conjugate.

2.3. Characterization method

TEM grids were prepared by applying a diluted drop of the ZnO samples to carbon-coated copper grids. The particle sizes were determined from micrographs recorded at a magnification of 100 000× using an FEI (Technais-Twin, operating at 200 kV) instrument. For optical experiments, the steady state absorption and emission were determined using a Shimadzu UV-2450 spectrophotometer and a Jobin Yvon Fluorolog, respectively. Picosecond-resolved spectroscopic studies were done using a commercial time correlated single photon counting (TCSPC) setup with MCP-PMT from Edinburgh Instruments (IRF = 80 ps) using a 375 nm excitation laser source. Details of the time resolved fluorescence setup have been depicted in our previous reports.[37–39] For FTIR study, a JASCO FTIR-6300 instrument of 0.5 cm^{-1} resolution was used. Raman scattering experiments were carried out by a Micro Raman setup (Horiba LabRAM) with the excitation wavelength of 532 nm at room temperature.

2.4. Preparation of dichlorofluorescein and ROS measurements

DCFH was prepared from DCFH-DA by mixing 0.5 ml of 1.0 mM DCFH-DA in methanol with 2.0 ml of 0.01 N NaOH. This de-esterification of DCFH-DA proceeded at room temperature for 30 min, and the mixture was then neutralized with 10 ml of 25 mM NaH_2PO_4, at pH 7.4. This solution was kept on ice in the dark until use. All the measurements were performed in a total volume of 2 ml water that contained 10 μl of DCFH solution, RSV, ZnO and RSV–ZnO.

$$\underset{\text{(non-fluorescent)}}{\text{DCFH-DA}} \xrightarrow[\text{by NaOH}]{\text{deesterification}} \underset{\text{(non-fluorescent)}}{\text{DCFH}} \xrightarrow[\text{species}]{\text{reactive oxygen}} \underset{\text{(fluorescent)}}{\text{DCF}}$$

2.5. Bacterial strain and culture condition

The viable count assay was performed with *E. Coli* XL1-blue cells. The cells were cultured at 37 °C in a liquid Luria–Bertani (LB) medium. When the optical density reached 0.6, the inoculums was serially diluted ten thousand times with a Luria–Bertani (LB) medium and plated in different plates containing RSV, ZnO NPs and RSV–ZnO. In order to study the effect of drugs, the plates were then incubated at 37 °C for 24 hours. Finally the colonies were counted after overnight incubation.

2.6. Cell culture

The human ovarian carcinoma cell lines (PA1) were cultured in EMEM medium supplemented with 10% fetal bovine serum (FBS) and 1% antibiotic at 37 °C in a humidified atmosphere of 95% air and 5% CO_2.

2.7. Cytotoxicity assays

(i) Cell viability assay. The cell viability assay was assessed using the MTT assay following the method of Mossmann.[40] The cells were incubated for 24 h with different concentration of RSV, ZnO NPs and RSV–ZnO and 3 hours with MTT [3-(4,5-dimethylthiozoyl-2-yl)-2,5-diphenyltetrazolium bromide] dye (5 mg ml^{-1} in PBS). The medium from each well was discarded and the resulting formazan crystals were solubilised by adding 150 μl of dimethyl sulphoxide and quantified by measuring absorbance at 530 nm in an Elisa Reader. Cytotoxicity has been stated as the concentration of corresponding substance as inhibitory cell growth factor by 50% (IC_{50}), and all tests and analyses were performed in triplicate. The IC_{50} value of ZnO NPs, RSV and RSV–ZnO nano-conjugate was calculated from MTT assay.

(ii) Determination of cell cycle by flow cytometry. Cell viability under CC_{50} value of RSV, ZnO NPs, and RSV–ZnO were analyzed on flow cytometer (FACS Calibur, Beckton Dickinson, SanJose). Cell cycle phase distribution of nuclear DNA was determined by PI fluorescence (excited with 488 nm argon laser light and detected the fluorescence at 623 nm) and analysed through CellQuest software (Becton-Dickinson, San Jose). Ten thousand total events were acquired and histogram display of DNA content (*x*-axis, PI fluorescence) *vs.* counts (*y*-axis) has been displayed.

2.8. Oxidative stress parameters

(i) Measurement of intracellular reactive oxygen species (ROS). The level of intracellular ROS generation was estimated by using 2,7-dichlorofluorescein diacetate (DCFDA) dye.[40] Cells were seeded in a 6-well black bottom plate (10^4 cells per well). After 24 hours, the cells were exposed to ZnO NPs, RSV, and RSV–ZnO nano-conjugate for up to 6 hours. Following exposure, the cells were washed twice with PBS and incubated with DCFDA dye (20 μM) for 30 minutes at 37 °C. The reaction mixture was then use to measure the fluorescence intensity by FACS. Intracellular ROS were measured by flow cytometric analysis as we have previously reported.[41]

(ii) Measurement of mitochondrial membrane depolarization. While the transition pore was partially functional, the functional dysfunction of the mitochondria was detected by measurement of membrane depolarization. To determine whether there was membrane dysfunction, JC-1 staining was performed by flow cytometry analysis. Mitochondrial membrane depolarization was detected with the fluorescent probe 5,5′,6,6′-tetrachloro-1,1′,3,3′-tetraethylbenzimidazolcarbocyanine iodide (JC-1). Mitochondrial energization was determined by retention of JC-1 dye.[42] Cells exposed to ZnO NPs, RSV and RSV–ZnO with their IC_{50} value were harvested by trypsinization and washed with PBS twice. The cells were incubated with 10 μM JC-1 for 15 minutes at 37 °C, washed with PBS and re-suspended in PBS at a concentration of 10^6 cells per ml. The fluorescence intensity was measured at an emission wavelength of 590 nm upon excitation wavelength at 485 nm using FACS.

2.9. Apoptosis

(i) Annexin V-FITC/PI staining. Annexin V-FITC/PI staining was carried out by Annexin V-FITC apoptosis detection kit as per the manufacturer's protocol. Briefly, the cells were harvested by trypsinization, washed with PBS and re-suspended in binding buffer at a concentration of 10^6 cells per ml. Annexin V-FITC (5 μl) and propidium iodide (10 μl) was added to 500 μl of cell suspension and incubated for 10 minutes in the dark at room temperature. The cells were immediately analyzed by FACS. Fluorescence emitted by Annexin V bound FITC and DNA-bound propidium iodide in each event was detected. Results were analyzed by FACSDiva 6.1.2 software.

(ii) Hoechst staining. Apoptotic nuclear morphology was also assessed using Hoechst 33342. Cells were fixed with 4% *para*-formaldehyde at room temperature for 30 minutes, and were washed with PBS and then stained with 10 μg ml^{-1} of Hoechst 33342 solution at 37 °C for 10 minutes. The cells were washed and the morphology was observed by fluorescence microscope.

2.10. Western blot

Human ovarian cancer PA1 cells were cultured in six-well plates and exposed to ZnO NPs, RSV and RSV–ZnO nano-conjugate at the concentration of CC_{50} value for 24 hours. The harvested cell pellets were lysed in lysis buffer (50 mM Tris HCl) in the presence of a protease inhibitor. The total protein concentration was measured by the Bradford method[45] bovine serum albumin as the standard. A 40 μg per lane protein were separated by 10% SDS–polyacrylamide gel electrophoresis and transferred onto a nitrocellulose blotting membrane (Bio-rad) for overnight. The membrane was blocked with 5% non fat milk for 1.5 hours at room temp and probed with anti-mouse primary antibody (1 : 1000) against beta-actin, Bcl-2, Bax, Caspase-9 for 1 hour at room temperature followed by overnight incubation at 4 °C. The membrane was then incubated for 1.5 hours at room temperature with secondary antibodies conjugated to horseradish peroxidise at 1 : 5000 dilution. The protein bands were visualised on X-ray film using an enhanced chemiluminescence system.

2.11. Statistical analysis

All quantitative data are expressed as mean ± SD unless otherwise stated. One-way analysis of variance followed by Tukey's multiple comparison test was executed for comparison of different parameters between the groups using a computer program GraphPad Prism (version 5.00 for Windows), GraphPad Software (CA, USA). $p < 0.05$ was considered significant.[43]

3. Result and discussion

3.1. Structural characterization of RSV–ZnO nano-conjugate

Fig. 1a depicts a characteristic HRTEM image of the ZnO NPs. From the lattice fringe of a single ZnO NPs, inter planar distance is found to be approximately 0.31 nm, which corresponds to the spacing between two (100) planes. The HRTEM image clearly reflects the crystalline nature of ZnO NPs.[44] The average particle size was determined from our experimental HRTEM data and found to be approximately 4.89 ± 0.5 nm as revealing from inset of Fig. 1a. The absorption spectra of ZnO NPs, RSV and RSV–ZnO nano-conjugate are shown in Fig. 1b. The major absorption peak of RSV appears at 327 nm with a shoulder at 311 nm. No distinct peak of RSV is observed in absorption spectra of nano-conjugate due to the very low concentration of RSV and large scattering of the ZnO NPs. The drug used in this study, RSV, contains three hydroxyl groups, which possesses binding ability to the surface of ZnO.[45] The Fourier transform infra-red (FTIR) technique is used to investigate the binding mode of the hydroxyl group of RSV on the ZnO surface. For the pure drug the stretching frequency of hydroxyl group is located at 3498 cm^{-1} as reported earlier. The peak observed at 3430 cm^{-1} is due to O–H stretching vibration of ZnO.[46] The perturbation of peak at 3498 cm^{-1} of RSV upon attached to ZnO as shown in Fig. 2a, is revealing that RSV is attached to ZnO NPs through O–H functional group. To further investigate the binding between the drug and delivery vehicle, Raman spectra were collected from RSV, ZnO NPs and

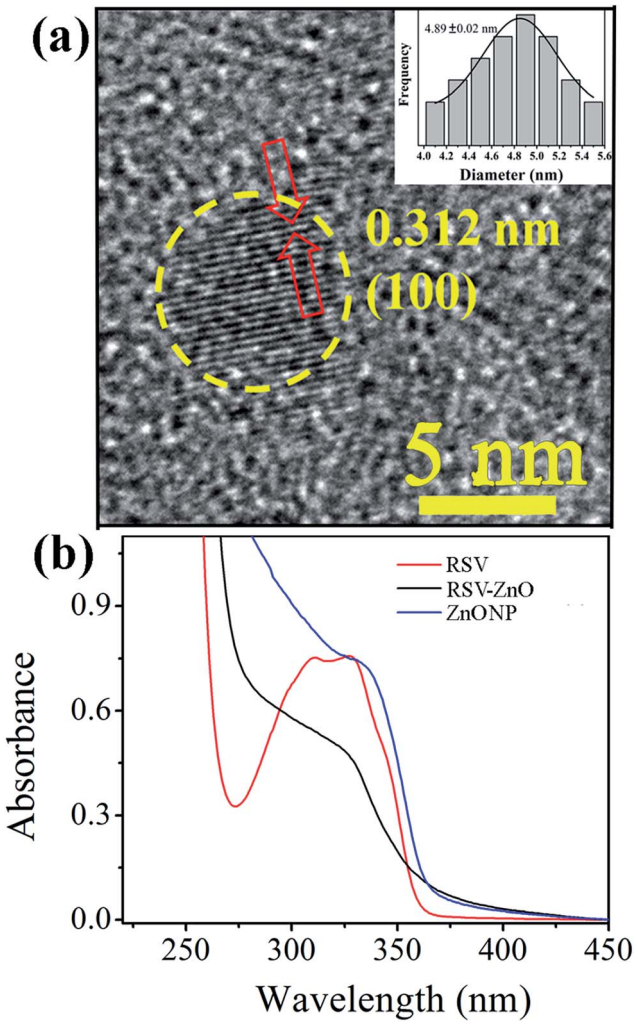

Fig. 1 (a) High-resolution TEM (HRTEM) image of ZnO NPs with. Inset shows the size distribution of the ZnO NPs (b) UV-vis absorption of ZnO NPs, RSV and RSV–ZnO.

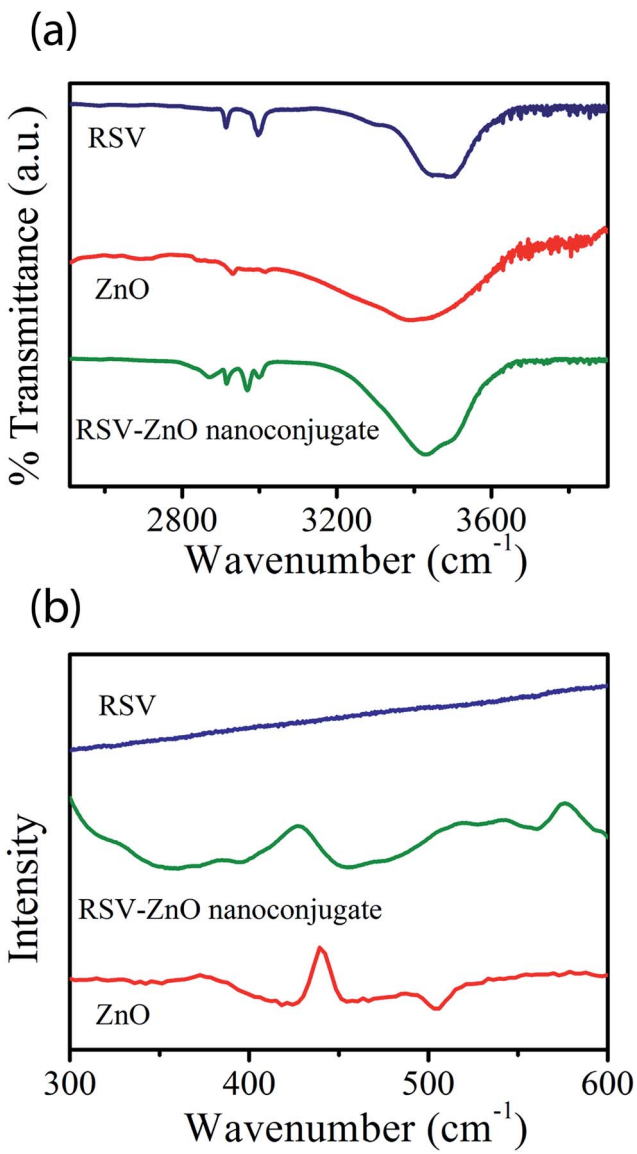

Fig. 2 (a) FTIR and (b) Raman spectra of RSV, ZnO NPs and RSV–ZnO nano-composites.

RSV–ZnO nano-conjugate as shown in Fig. 2b. The Raman spectrum of RSV does not show any peak in the wavenumber range of 300–600 cm^{-1}. However, four vibration peaks at 328, 378, 438, and 577 cm^{-1} are observed in the Raman spectrum of ZnO NPs as reported earlier.[47,48] The strong peak at 438 cm^{-1} is corresponds to the nonpolar optical phonon, E_2 mode of the ZnO NPs at high frequency, which is associated with oxygen deficiency. After binding to RSV, the peak at 438 cm^{-1} of ZnO is significantly perturbed. This is indicative of the passivation of ZnO surface states upon RSV assembly. The presence of other characteristic bands indicates good retention of ZnO crystal structure and shape during the sensitization of ZnO NPs with RSV.

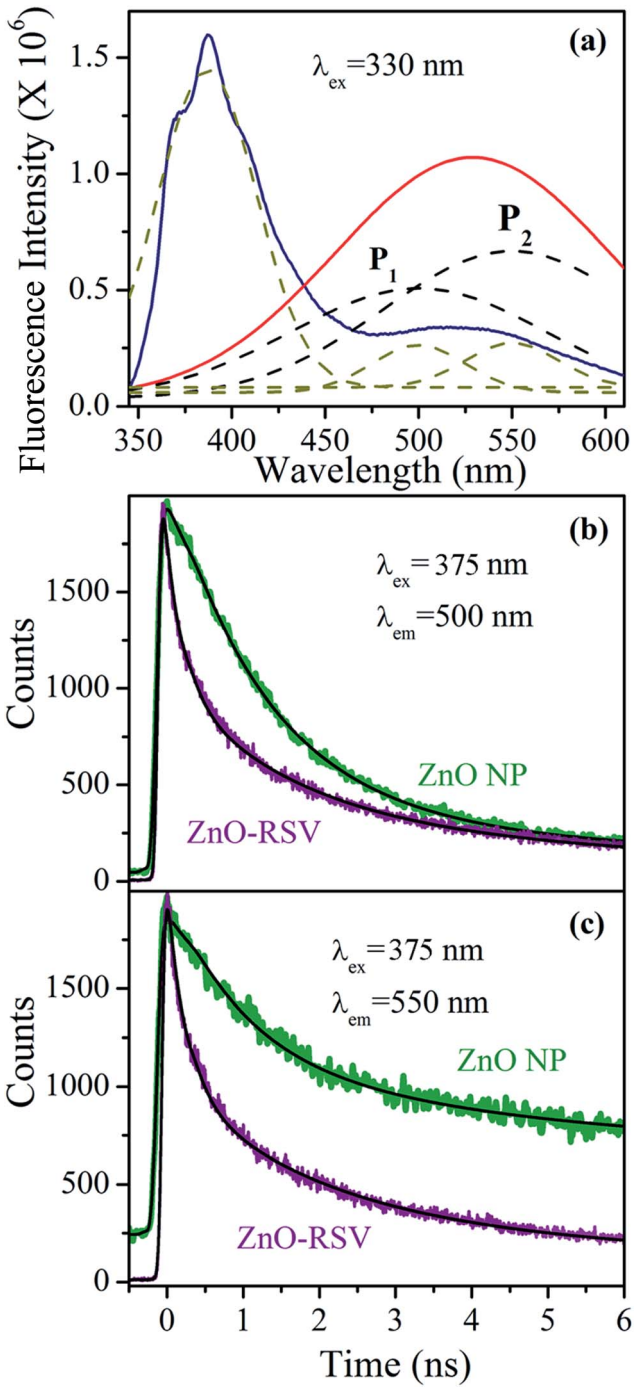

Fig. 3 (a) Fluorescence spectra of ZnO NPs and RSV–ZnO nanocomposites are shown. The broad emission band is composed of two components, P1 (500 nm) and P2 (550 nm). The picosecond-resolved fluorescence transients of ZnO NPs (excitation at 375 nm) in the absence and in the presence of RSV collected at (b) 500 nm and (c) 550 nm are shown.

3.2. Steady-state and picosecond-resolved fluorescence study

As shown in Fig. 3a the room temperature steady-state emission of ZnO NPs is very broad around 530 nm upon excitation above the band-edge (λ_{ex} = 330 nm) due to presence of defect states near the surface of ZnO. The broad emission is composed of two emission band 500 nm (P1) and 550 nm (P2).[49] While the first one corresponds to singly charged vacancy center V_0^+, the other one is arising due to doubly charged vacancy center V_0^{++}. The emission intensity of ZnO NPs in the RSV–ZnO nanoconjugate decreases considerably than that of free ZnO NPs which can be attributed to the efficient electron transfer processes from ZnO NPs to RSV. To investigate the mechanism we have extended our study with picosecond resolved fluorescence spectroscopy. The fluorescence decay profile of ZnO NPs in the presence and absence of RSV was obtained upon excitation of a 375 nm laser and monitored at 500 nm (P1) and 550 nm (P2) (Fig. 3b and c, respectively). The excited state lifetime of the ZnO NPs quenches in the RSV–ZnO nanohybrid compared to that of free ZnO NPs. The details of the spectroscopic parameters and the fitting parameters of the fluorescence decays are tabulated in Table 1. The faster component in RSV–ZnO nano-conjugates is compared with the earlier study of ZnO–benzoquinone (BQ), efficiently accepts excited electrons from the surface of semiconductor quantum dots.[50] Similar time scales reveal the excited state electron transfer from ZnO NPs to RSV.

3.3. *In vitro* ROS activity

After investigation of the interfacial dynamics and molecular proximity, we have extended our studies to the anti-microbial activity of RSV–ZnO composite. RSV exhibits anticancer effect on various human cancer cells through ROS. However, due to low solubility of RSV in water the anticancer efficacy decreases. In this juncture we have used RSV–ZnO nano-conjugates as a potential antibacterial agent for the inhibition of growth of *Escherichia coli* (*E. coli*). The upper panel of Fig. 4a shows picture of *E. coli* cultures treated with DMSO, ZnO NPs, RSV

Table 1 Fluorescence lifetimes (τ_i) of different systems in two detection wavelengths 500 nm and 550 nm (λ_{ex} = 375 nm)

System	τ_1 ns (%)	τ_2 ns (%)	τ_3 ns (%)	τ_{avg} ns
ZnO NPs (em@500 nm)	1.15 (70)	2.45 (25)	38.67 (5)	3.35
ZnO NPs (em@550 nm)	0.96 (51)	3.94 (21)	44.81 (28)	13.86
RSV–ZnO (em@500 nm)	0.19 (58)	1.63 (31)	9.13 (12)	1.17
RSV–ZnO (em@550 nm)	0.21 (59)	1.86 (29)	10.99 (12)	1.98

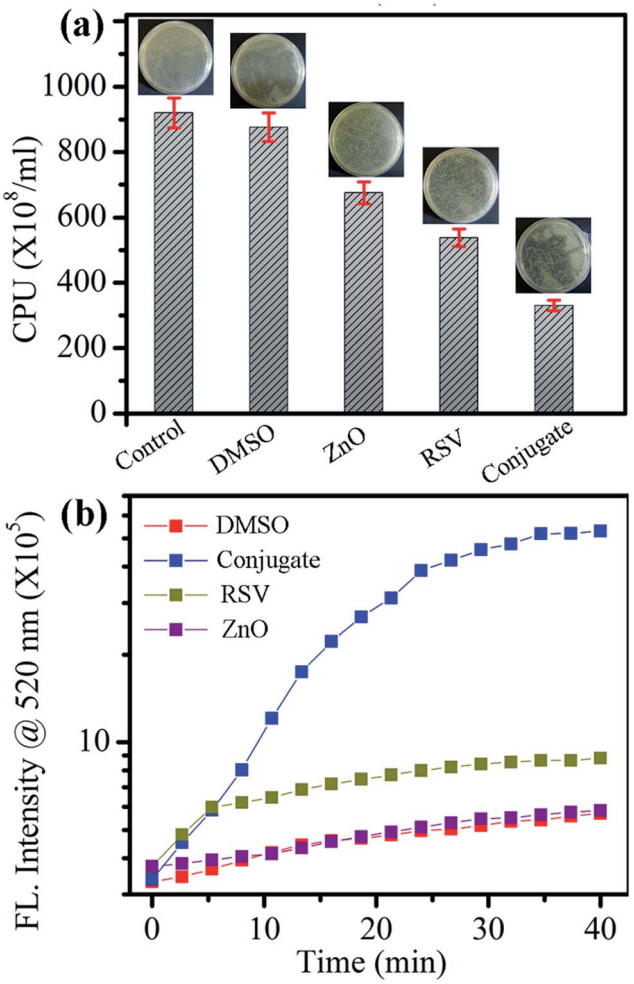

Fig. 4 (a) Antibacterial activity of RSV–ZnO, RSV and ZnO. The upper panel shows images of *E. coli* plates in presence of the corresponding samples. (b) The DCFH oxidation with time in the presence of RSV–ZnO, RSV and ZnO and DCFH only.

and RSV–ZnO nano-conjugate. The inhibition in growth of the bacterial culture for RSV–ZnO nano-conjugates is clearly visible. The culture treated with RSV–ZnO nano-conjugate contains a smaller number of colonies with respect to the control samples and cultures containing ZnO NPs and RSV. The decrease of colony forming unit (CFU) is 65% in case of RSV–ZnO nano-conjugate as shown in Fig. 4a. In order to explain the detailed mechanistic view of both antioxidant and antimicrobial action of RSV–ZnO nano-conjugate, the ROS generation was investigated directly by dichlorofluorescin–dichlorofluorescein (DCFH–DCF) conversion in aqueous medium. DCFH is a widely known marker that is used in ROS detection assays.[51,52] The ROS generated in the medium, oxidized non-fluorescent DCFH into fluorescent DCF. The fluorescence emission intensity of DCF was monitored with respect to time. As RSV itself generates some ROS, there is some enhancement in fluorescence intensity of DCFH as shown in the Fig. 4b. However, maximum enhancement of fluorescence intensity in case of RSV–ZnO nano-conjugate compared to free RSV as shown in Fig. 4b. A control experiment was performed where ZnO NPs and DCFH only show negligible ROS generation.

3.4. *In vitro* cytotoxicity

The strategy of investigating cytotoxicity in different cell lines using MTT is well documented in the literature.[53,54] We have performed MTT assay on the ovarian cancer cell line (PA1) to

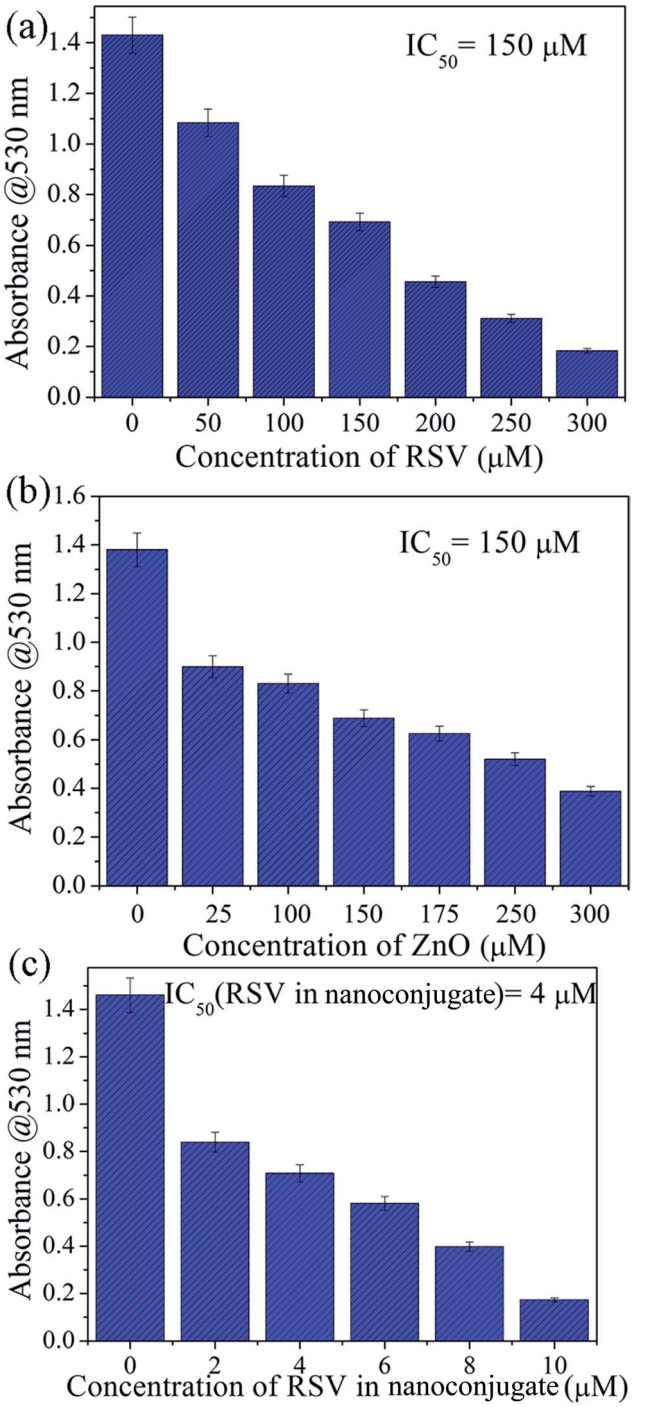

Fig. 5 Cells were treated with different concentration of RSV, ZnO NPs and RSV–ZnO nano-conjugate for 24 h. Viability was quantified by MTT assay.

investigate the cytotoxicity of RSV–ZnO nano-conjugates with respect to its precursors, RSV and ZnO NPs. IC_{50} values for RSV, ZnO are 150 μM for both in PA1 cell line. However, for RSV–ZnO nano-conjugate the IC_{50} value is 4 μM and 100 μM for individual concentration of RSV and ZnO in nano conjugate, respectively. Clearly, the assay revealed a much high cytotoxic potential of the nano-conjugate compare to that of RSV only on PA1 cell line as shown in Fig. 5. In Fig. 6 we have also represented the morphological change of cells after treatment by phase contrast microscopy. Additionally our findings also estimate that conjugate creates potent toxicity in PA1 cells more efficiently than that of RSV. In order to compare the potent toxicity effect of RSV–ZnO compared to RSV on PA1 cells, we performed the flow cytometric cell cycle phase distribution analysis. As shown in Fig. 7, our results showed significant higher cell death of PA1 cell line with the treatment of RSV–ZnO at even lower dose in compare to that of RSV. Conjugate generate 41.74% cell death compare to 30.98% with RSV treatment and ZnO NPs separately generate 13.34% of cell death at same concentration.

3.5. Induction of apoptosis

To confirm the findings obtained from MTT assay we performed phase contrast microscopic imaging of PA1 cells on treatment with RSV, ZnO NPs and RSV–ZnO nano-conjugate as shown in Fig. 6. Our observation showed that nano-conjugate produced similar percentage (50%) of cell death at a lower concentration (4 μM RSV individual concentration in the nano-conjugate) compare to RSV and highlighting that the efficacy of conjugate to induce death in PA1 cells was superior to that of RSV.

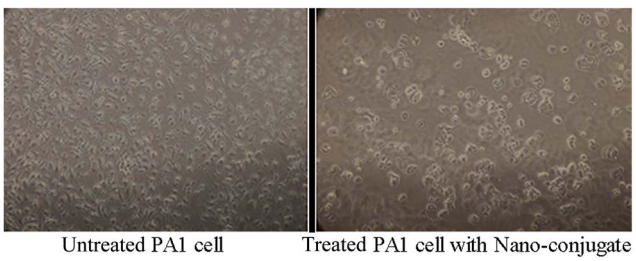

Fig. 6 Cell morphology change after treatment by phase contrast microscopy.

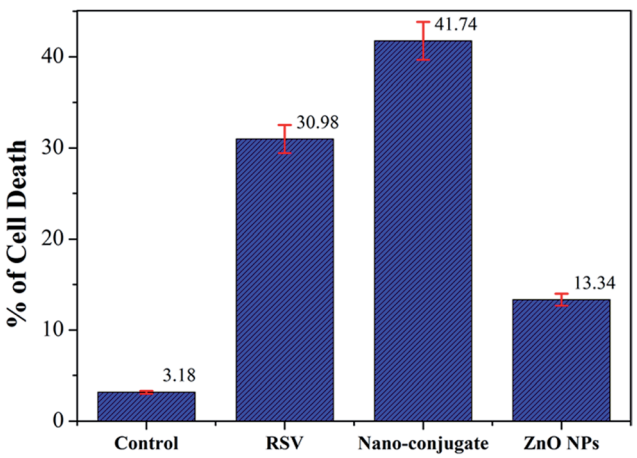

Fig. 7 Sub G_0 value of samples which describe the % of cell death by apoptosis in cell cycle study.

To further assess whether the cell death was due to apoptosis or not we examined the percentage of Annexin-V positive cells by flow cytometry. Flow cytometry analysis was conducted using Annexin V-FITC/PI staining to investigate the mode of cell death induced by RSV, ZnO NPs and RSV–ZnO. PA1 cells were treated with IC_{50} value of RSV, ZnO and RSV–ZnO for 24 h. The cells treated with RSV, ZnO and RSV–ZnO for 24 hours showed 50.22%, 19.81% and 62.74% apoptotic cells, respectively (Fig. 8). Apoptosis was further confirmed by Hoechst 33342 staining. PA1 cells were treated by RSV and RSV–ZnO nano-conjugate for 24 hours and examined for nuclear morphology along with a control. As revealed from Fig. 9 treated cells showed marked DNA condensed nuclei and apoptotic bodies whereas control cells had homogenously stained nuclei.

3.6. Induce apoptosis *via* ROS generation targeting mitochondria mediated pathway

It is well established and also supported by many scientific reports that high level of ROS formation usually inhibit the proliferation of many types of cells[55] and RSV has been identified as a potent antioxidant that can promote ROS generation.[56] So in the present experimental set up we first evaluated whether treatment with conjugate could up regulate the formation of ROS higher than the RSV only in PA1 cells were treated with IC_{50} value of RSV and nano-conjugate with different time interval (0, 10 minutes, 30 minutes, 1 h, 2 h, 4 h and 6 h). The generated ROS was measured using the fluorescence dye DCFH-DA and the results were analyzed using flow cytometry. Treatment with conjugate produce much higher ROS with lower concentration in compare to that of RSV in PA1 cells as shown in Fig. 10. Apparently both the ZnO and RSV promoted the formation of ROS in time dependent manner but conjugate was found to efficiently increase ROS generation at significant lower dose than RSV.

After estimation of ROS generation in PA1 cells by conjugate treatment, we analyzed the mitochondrial membrane depolarization in treated cells and found a change of mitochondrial membrane potential in PA1 cells. Fig. 11 reveals the cells treated with RSV, ZnO NPs and RSV–ZnO for 6 h showed a marked increase ($p < 0.05$ compared to control in all cases) in percentage of depolarized cell number. There were 35% depolarized cells at IC_{50} value of RSV–ZnO as compared to the control cells. The value of depolarised cells in case of RSV–ZnO is significantly differ from RSV ($p < 0.0024$) and ZnO NPs ($p < 0.002$) treated systems. The taken together our findings suggest that conjugation induced apoptosis is also mediated through ROS generation and have much effect on PA1 cell line.

3.7. Analysis of key apoptotic protein

Apoptosis can be initiated by intracellular and extracellular signals that determine whether a cell is to survive or undergo apoptosis. In previous findings it has been shown that Bcl-2

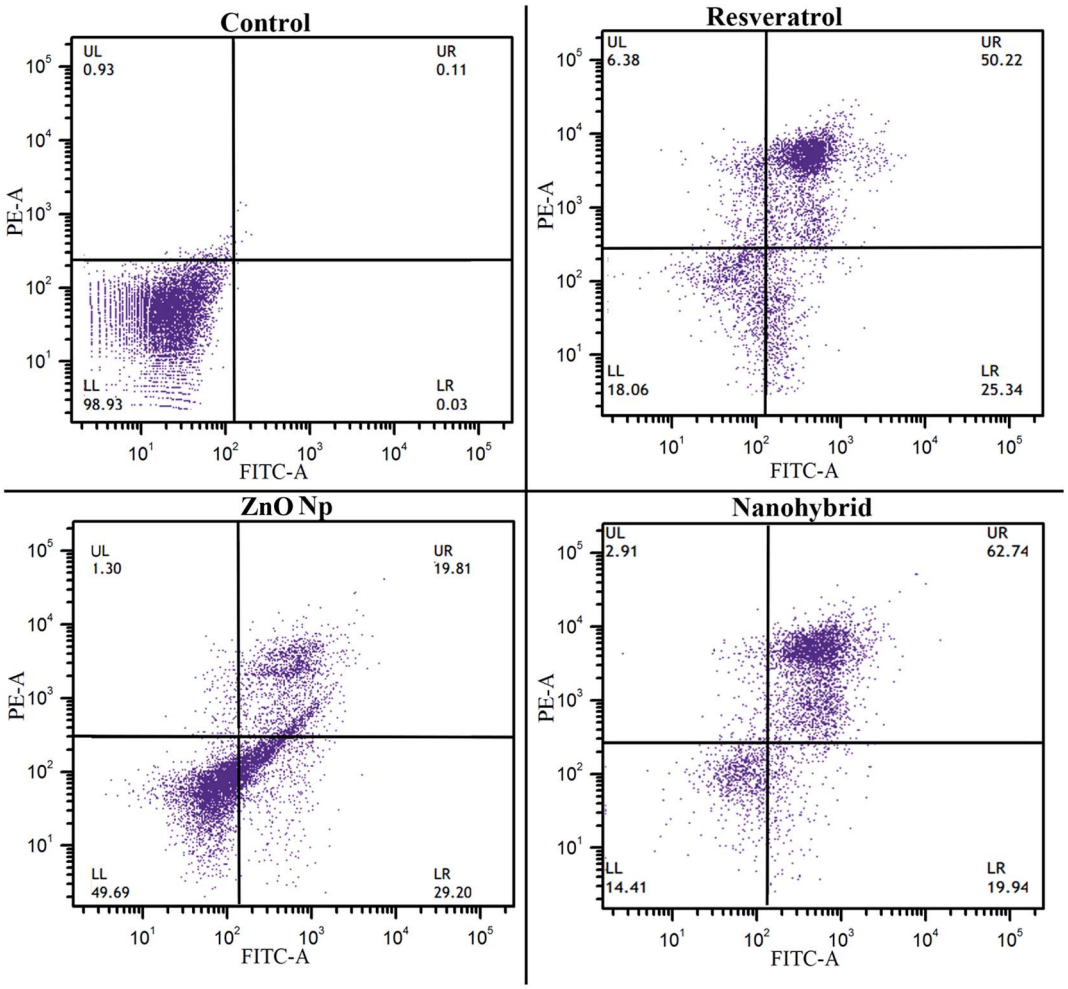

Fig. 8 RSV, ZnO, RSV–ZnO induced apoptosis in PA1 cells: flow cytometric analysis of Annexin V-FITC/PI stained cells representative dot plots of four independent experiments are presented.

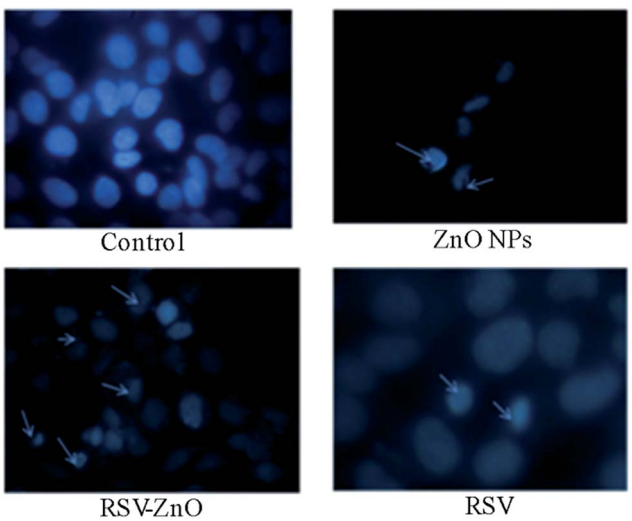

Fig. 9 Fluorescence image of cells stained with Hoechst 33342. RSV, ZnO and RSV–ZnO treated cells show apoptotic cells with condensed or fragmented nuclei (indicated by arrow).

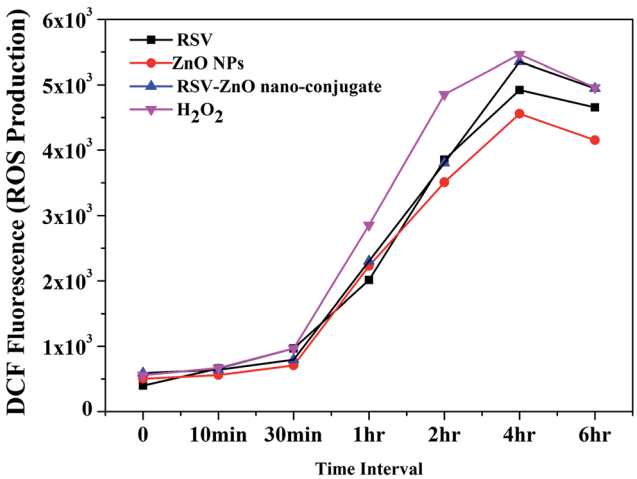

Fig. 10 RSV, ZnO, RSV–ZnO treated cells were assessed by flow cytometry for ROS generation by measuring DCF-fluorescence intensity and the data was represented as line diagram.

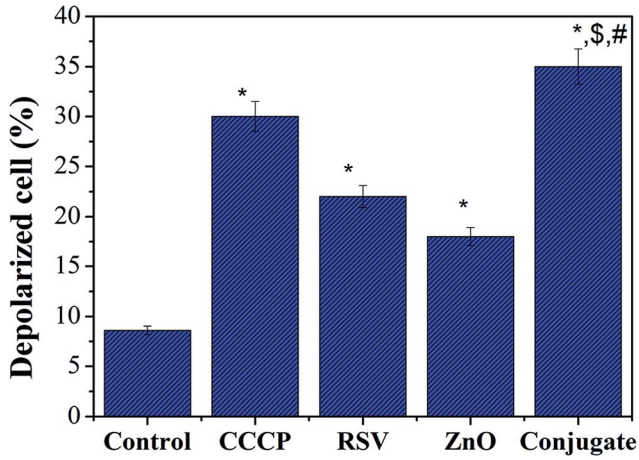

Fig. 11 Flow cytometric analysis of JC-1 stained cells to study mitochondrial membrane potential changes. RSV–ZnO treated cells show high mitochondrial membrane depolarization in compare to control, RSV, and ZnO respectively. *Values differ significantly from control ($p < 0.005$), $^{\$}$value of conjugate differ significantly from RSV ($p < 0.002$), $^{\#}$value of conjugate differ significantly from ZnO ($p < 0.002$).

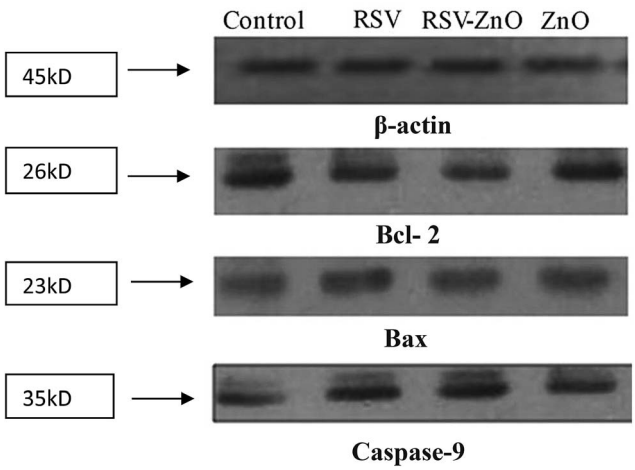

Fig. 12 Western blot analysis of proteins involved in apoptosis: Bax, Bcl-2, and Caspase-9 proteins in PA1 cells treated with RSV, RSV–ZnO and ZnO with their IC_{50} concentration for 24 h. β-Actin was used as control.

family members are the mediators of cell survival and apoptosis. The expression level of key apoptotic protein was examined in treated cells by western blotting. Fig. 12 reveals a significant increase in Bax protein expression level and decrease level of Bcl-2 protein expression infers the apoptosis pathway of ovarian cancer cell death.[57,58] For further confirmation, we have also performed the expression level of Caspase 9 protein in PA1 cells upon treatment with RSV ZnO NPs and RSV–ZnO nano-conjugate. A significant increase in Caspase-9 levels was revealed from our study. Bax and Bcl-2 are pro and anti apoptotic proteins, respectively and Caspase-9 is also an apoptotic protein.[59] Our results strongly suggest that lose dose conjugate inhibits ovarian cancer cell growth *via* apoptosis mechanism as shown in Scheme 1.

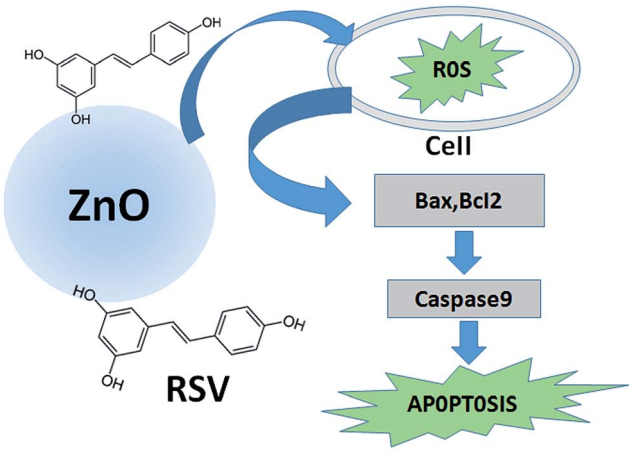

Scheme 1 Schematic representation of apoptotic cell death of cancer cell through enhanced ROS generation of ZnO–RSV composite inside the ovarian cancer cell.

4. Conclusion

In summary, we have investigated the enhanced efficacy of RSV–ZnO nano-conjugate over free RSV in PA1 cells (ovarian cancer cell). Also we have explored different mechanism like cytotoxicity, oxidative stress parameters and apoptosis in same cells upon treatment with RSV–ZnO nano-conjugate. The RSV–ZnO nano-conjugate was characterized by FTIR spectroscopy, Raman scattering and TEM images. Picosecond-resolved fluorescence studies on RES–ZnO nano-conjugate also reveal efficient electron migration from ZnO to RSV, eventually enhancing the ROS activity in the RSV–ZnO nano-structures. PA1 cells exposed with IC_{50} value of drugs which showed decrease in cell viability and the mode of induced cell death was found to be apoptosis and the percentage of apoptosis is higher than free RSV. RSV–ZnO nano-conjugate also induced high oxidative stress by ROS generation than free RSV. Mitochondrial membrane depolarization value is also high in case of RSV–ZnO nano-conjugate than free RSV. Our results evaluate that apoptosis is occurred through high ROS generation and mitochondrial membrane depolarization. Our findings reveal that the RSV–ZnO nano-conjugate shows much more efficacy in anticancer effect on PA1 cells compare to free RSV.

Acknowledgements

M. K. thanks Maulana Azad National fellowships (MANF), UGC, India and S. C. thanks CSIR, India for their research fellowships. PL thanks the Braunschweig International Graduate School of Metrology B-IGSM and the DFG Research Training Group GrK 1952/1 “Metrology for Complex Nanosystems” for support. We thank UGC-CAS for central instrumental facility of University of Calcutta. We also thank DST (India) for financial grants (SB/S1/PC-011/2013) and DAE (India) for (2013/37P/73/BRNS).

References

1 N. Colombo, T. Van Gorp, G. Parma, F. Amant, G. Gatta, C. Sessa and I. Vergote, *Critical reviews in oncology/hematology*, 2006, **60**, 159–179.
2 T. J. Herzog and B. Pothuri, *Nat. Clin. Pract. Oncol.*, 2006, **3**, 604–611.
3 G. D. Aletti, M. M. Gallenberg, W. A. Cliby, A. Jatoi and L. C. Hartmann, *Mayo Clin. Proc.*, 2007, **6**, 751–770.
4 V. R. Martin, *Clin. J. Oncol. Nurs.*, 2007, **11**, 201.
5 M. Fung-Kee-Fung, T. Oliver, L. Elit, H. W. Hirte and P. Bryson, *Curr. Oncol.*, 2007, **14**, 195–208.
6 M. Campagna and C. Rivas, *Biochem. Soc. Trans.*, 2010, **38**, 50–53.
7 S. Das and D. K. Das, *Recent Pat. Cardiovasc. Drug Discovery*, 2007, **2**, 133–138.
8 T. Richard, A. D. Pawlus, M. L. Iglésias, E. Pedrot, P. Waffo-Teguo, J. M. Mérillon and J. P. Monti, *Ann. N. Y. Acad. Sci.*, 2011, **1215**, 103–108.
9 M. Jang, L. Cai, G. O. Udeani, K. V. Slowing, C. F. Thomas, C. W. Beecher, H. H. Fong, N. R. Farnsworth, A. D. Kinghorn and R. G. Mehta, *Science*, 1997, **275**, 218–220.
10 P. B. Tze-Chenhsieh, J. M. Ketanlaud, F. Traganos, Z. Darzynkiewicz and J. M. Wu, *Int. J. Oncol.*, 1999, **15**, 245–252.
11 J. Dörrie, H. Gerauer, Y. Wachter and S. J. Zunino, *Cancer Res.*, 2001, **61**, 4731–4739.
12 Z. Chen, K. Jin, L. Gao, G. Lou, Y. Jin, Y. Yu and Y. Lou, *Eur. J. Pharmacol.*, 2010, **643**, 170–179.
13 N. Oi, C.-H. Jeong, J. Nadas, Y.-Y. Cho, A. Pugliese, A. M. Bode and Z. Dong, *Cancer Res.*, 2010, **70**, 9755–9764.
14 M. Sengottuvelan, P. Viswanathan and N. Nalini, *Carcinogenesis*, 2006, **27**, 1038–1046.
15 S. H. Mitchell, W. Zhu and C. Y. Young, *Cancer Res.*, 1999, **59**, 5892–5895.
16 A. W. Opipari, L. Tan, A. E. Boitano, D. R. Sorenson, A. Aurora and J. R. Liu, *Cancer Res.*, 2004, **64**, 696–703.
17 I. Zoberi, C. M. Bradbury, H. A. Curry, K. S. Bisht, P. C. Goswami, J. L. R. Roti and D. Gius, *Cancer Lett.*, 2002, **175**, 165–173.
18 K. W. Lee, A. M. Bode and Z. Dong, *Nat. Rev. Cancer*, 2011, **11**, 211–218.
19 M. E. l. Juan, J. Buenafuente, I. Casals and J. M. Planas, *Food Res. Int.*, 2002, **35**, 195–199.
20 P. Signorelli and R. Ghidoni, *J. Nutr. Biochem.*, 2005, **16**, 449–466.
21 V. Sanna and M. Sechi, *Maturitas*, 2012, **73**, 27–32.
22 S. John, S. Marpu, J. Li, M. Omary, Z. Hu, Y. Fujita and A. Neogi, *J. Nanosci. Nanotechnol.*, 2010, **10**, 1707–1712.
23 H. Yang, C. Liu, D. Yang, H. Zhang and Z. Xi, *J. Appl. Toxicol.*, 2009, **29**, 69–78.
24 K. Gerloff, C. Albrecht, A. W. Boots, I. Forster and R. P. F. Schins, *Nanotechnology*, 2009, **3**(4), 355–364.
25 T. Jin, D. Sun, J. P. Su, H. Zhang and H. J. Sue, *J. Food Sci.*, 2009, **74**(1), 46–52.
26 J. W. Rasmussen, E. Martinez, P. Louka and D. G. Wingett, *Expert Opin. Drug Delivery*, 2010, **7**(9), 1063–1077.
27 S. John, S. Marpu, J. Li, M. Omary, Z. Hu, Y. Fujita, *et al.*, *J. Nanosci. Nanotechnol.*, 2010, **10**(3), 1707–1712.
28 A. Gojova, B. Guo, R. S. Kota, J. C. Rutledge, I. M. Kennedy and A. L. Barakal, *Environ. Health Perspect.*, 2007, **115**(3), 403–409.
29 H. Yang, C. Liu, D. Yang, H. Zhang and Z. Xi, *J. Appl. Toxicol.*, 2009, **29**, 69–78.
30 I. F. Osman, A. Baumgartner, E. Cemeli, J. N. Fletcher and D. Anderson, *Nanomedicine*, 2010, **5**(8), 1193–1203.
31 S. George, S. Pokhrel, T. Xia, B. Gillbert, Z. Ji, M. Schowalter, *et al.*, *ACS Nano*, 2009, **4**(1), 15–29.
32 N. M. Franklin, N. J. Rogers, S. C. Apte, G. E. Batley, G. E. Gadd and P. S. Casey, *Environ. Sci. Technol.*, 2007, **41**(24), 8484–8490.
33 P. J. Moos, K. Chung, D. Woessner, M. Honeggar, N. S. Cutler and J. M. Vernath, *Chem. Res. Toxicol.*, 2010, **23**(4), 733–739.
34 J. Cadet, T. Douki and J. L. Ravanat, *Free Radical Biol. Med.*, 2010, **49**(1), 9–21.
35 J. Neuzil, X. F. Wang, L. F. Dong, P. Low and S. Ralph, *FEBS Lett.*, 2006, **580**(22), 5125–5129.
36 S. Sarkar, A. Makhal, T. Bora, S. Baruah, J. Dutta and S. K. Pal, *Phys. Chem. Chem. Phys.*, 2011, **13**, 12488–12496.
37 S. Choudhury, S. Batabyal, T. Mondol, D. Sao, P. Lemmens and S. K. Pal, *Chem.–Asian J.*, 2014, **9**, 1395–1402.
38 S. Choudhury, P. K. Mondal, V. Sharma, S. Mitra, V. G. Sakai, R. Mukhopadhyay and S. K. Pal, *J. Phys. Chem. B*, 2015, **119**, 10849–10857.
39 S. Choudhury, B. Ghosh, P. Singh, R. Ghosh, S. Roy and S. K. Pal, *Phys. Chem. Chem. Phys.*, 2016, **18**, 17983–17990.
40 T. Mosmann, *J. Immunol. Methods*, 1983, **65**, 55–63.
41 C. P. Wan, E. Myung and B. H. Lau, *J. Immunol. Methods*, 1993, **159**, 131–138.
42 S. Shankar, X. Chen and R. K. Srivastava, *Prostate*, 2005, **62**, 165–186.
43 A. Adhikari, N. Polley, S. Darbar, D. Bagchi and S. K. Pal, *Future Sci. OA*, 2016, 1–21.
44 G. Darabdhara, P. K. Boruah, P. Borthakur, N. Hussain, M. R. Das, T. Ahamad, S. M. Alshehri, V. Malgras, K. C.-W. Wu and Y. Yamauchi, *Nanoscale*, 2016, **8**, 8276–8287.
45 H. Noei, H. Qiu, Y. Wang, E. Löffler, C. Wöll and M. Muhler, *Phys. Chem. Chem. Phys.*, 2008, **10**, 7092–7097.
46 S. Sarkar, A. Makhal, T. Bora, K. Lakhsman, A. Singha, J. Dutta and S. K. Pal, *ACS Appl. Mater. Interfaces*, 2012, **4**, 7027–7035.
47 W. Tu, J. Lei, P. Wang and H. Ju, *Chem.–Eur. J.*, 2011, **17**, 9440–9447.
48 Y. Zhang, H. Jia, R. Wang, C. Chen, X. Luo, D. Yu and C. Lee, *Appl. Phys. Lett.*, 2003, **83**, 4631–4633.
49 S. Sardar, S. Chaudhuri, P. Kar, S. Sarkar, P. Lemmens and S. K. Pal, *Phys. Chem. Chem. Phys.*, 2015, **17**, 166–177.
50 A. Makhal, S. Sarkar, T. Bora, S. Baruah, J. Dutta, A. Raychaudhuri and S. K. Pal, *J. Phys. Chem. C*, 2010, **114**, 10390–10395.

51 C. P. LeBel, H. Ischiropoulos and S. C. Bondy, *Chem. Res. Toxicol.*, 1992, **5**, 227–231.
52 D. Bagchi, S. Chaudhuri, S. Sardar, S. Choudhury, N. Polley, P. Lemmens and S. K. Pal, *RSC Adv.*, 2015, **5**, 102516–102524.
53 A. Dhawan and V. Sharma, *Anal. Bioanal. Chem.*, 2010, **398**, 589–605.
54 N. Monteiro-Riviere, A. Inman and L. Zhang, *Toxicol. Appl. Pharmacol.*, 2009, **234**, 222–235.
55 V. Sanna, A. M. Roggio, S. Siliani, M. Piccinini, S. Marceddu, A. Mariani and M. Sechi, *Int. J. Nanomed.*, 2012, **7**, 5501–5516.
56 G. Barrera, *ISRN Oncol.*, 2012, **2012**, 137289.
57 S. Cory and J. M. Adams, *Nat. Rev. Cancer*, 2002, **2**, 647–656.
58 G. Kroemer, *Nat. Med.*, 1997, **3**, 614–620.
59 G. Kroemer and S. J. Martin, *Nat. Med.*, 2005, **11**, 725–730.